Proceedings World Geothermal Congress 2020+1
Reykjavik, Iceland, April - October 2021

Chip-Hold-Down Effect on Rate-of-Penetration During Deep Percussive Drilling: A Theoretical Approach

Gaspar Gohin, Trond H. Bergstrøm, Marion Fourmeau, and Alexandre Kane

SINTEF, Post Box 4765 Torgarden, NO-7465 Trondheim

alexandre.kane@sintef.no

Keywords: percussive drilling; chip hold down; rock strengthening; drilling fluid; rate-of-penetration

ABSTRACT

A key issue in deep hard rock drilling is the decrease of rate-of-penetration (ROP) with depth. For rotary drilling, extensively used in the oil and gas sector, well-recognized causes for ROP decrease are rock strengthening and chip-hold-down effects. For percussive drilling, mainly used in the mining sector, the field data and theoretical analyses for deep well drilling are more limited. By analogy, the combined effect of rock strengthening and chip-hold-down on ROP is investigated here. Firstly, a fluid dynamic study of the removal of one rock chip is treated as a 2D fluid-structure interaction problem with an impermeable rock and incompressible drilling fluid. In particular, the mechanisms are the fluid infiltration and the stiction under the chip. Secondly, a stochastic ROP evaluation is developed using (i) a chip shape and size distribution and (ii) a condition for chip regrinding based on the characteristic times from the chip removal study. The ROP predictions are in good agreement with field data from the literature and the influence of chip geometry and fluid parameters is evaluated. These results provide input on the importance of tool, drilling and fluid parameters on the ROP, and can support the innovation and technology developments in percussive drilling.

1. INTRODUCTION

The high cost of drilling deep wells in hard rock formations is identified as the main cost driver and bottleneck for deep drilling applications. For instance, estimates show that the cost associated with drilling and well construction may reach 80 % of the upfront plant investments for deep geothermal energy exploitation, when using conventional drilling technologies (IEA Technology roadmap (2011)). Reduction in drilling costs can be pursued by modifying existing classical drilling technologies, or by developing novel solutions. New technologies such as high frequency hydraulic (and/or electric) percussion (and/or hybrid) drilling systems show high potential for cost-efficient ROP (Wittig et al. (2015)). The drilling process can be viewed structurally as a chain of technical challenges, among which the rock breaking and transport are probably the most important parts. The challenges frequently associated with hard rock drilling are for instance: low penetration rates, rapid wear and failure of drill bit.

An extensive literature is available on the decrease of ROP with depth using rotary drilling (drag bit, roller cone) [Garnier and Van Lingen (1959), Smith (1998), Andersen et al. (1990), Finger and Blankenship (2010), Hareland and Hoberock (1993), Rastegar et al. (2008), Warren (1987)]. For instance, as illustrated in Fig. 1a, Garnier and Van Lingen (1959) observed a decrease of 60 % of ROP using rotary drilling on 100 kg/cm^2, i.e. approximately 1000 m of mud fluid column, with various types of rock. They explained this drop with fluid pressure as a combination of rock strengthening (RS) effect and chip-hold-down (CHD) effect. The RS effect corresponds to the generally observed strength and ductility increase of rock material with confined stress states (Hoek and Brown (1980)). This results in a larger force applied on the cutter with depth, and consequently to a smaller depth of cut (for same amount of energy provided to the drill bit) for each cutter. The CHD effect is a phenomenon where the drilling fluid hydrostatic pressure hinders the rock chips from being removed from the bedrock by flushing. As a result, re-cutting of the chips occurs and the ROP decreases [Mitchell (2007), Niu (2010), Zhu et al. (2014)].

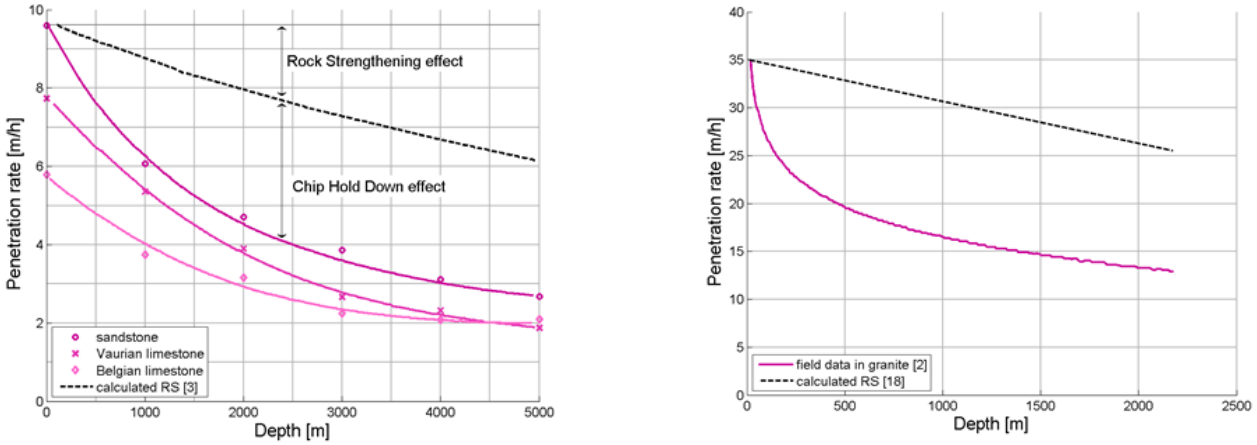

(a) (b)

Figure 1: ROP evolution with depth for (a) laboratory rotary drilling (from Garnier and Van Lingen (1959)) and (b) field percussive drilling in granite formation (Wittig et al. (2015))

Percussive (or hammer) drilling is generally used when hard formations are encountered, by repeated application of a large impulsive force to a continuously rotating drill bit by a hammer located on top of the drill bit (Depouhon (2014)). During the impact between the drill bit and the rock, the kinetic energy of the hammer is transformed into a deformation energy of the rock, leading to the bit penetration by indentation, crushing, and chipping of the rock. The efficiency of the percussive process relies on a combination of the drilling parameters (Fourmeau et al. (2015)) (i.e. impact energy, RPM, impact frequency). While it is recognized for its good efficiency in shallow wells, a non-linear decrease of ROP that reaches 50 % at 1000 m depth is reported with water percussion drilling in granite rock (Wittig et al. (2015)) (see Fig. 1b). However, available data and theoretical or numerical studies are very limited in the case of percussive drilling.

Percussive drilling technology with indentation takes advantage of the weak properties of the rock in tension to generate side cracks and chipping, in addition to the crushing of the high compressive area under the indenters (Tan et al. (1998)). The increased hydrostatic pressure with depth reduces the beneficial effect of tensile cracks and associated chipping. Simulations of single impacts with a multiple-buttons bit with both hydrostatic and lateral pressures show that at 100 MPa pressure level, the ROP, assumed proportional to damaged rock volume below the bit, decreased substantially compared to pressure free simulations: 38 % with hydrostatic pressure and 56 % with lateral pressure (Saksala (2016)). The cause of this reduction in rock damage (and corresponding ROP) is the compressive stress state, which prevents tensile and shear fractures. Percussive drilling field tests have also shown a correlation between the decrease of ROP and the decrease in mean cutting size (Altindag (2004)). However, the RS effect can only explain a ROP decrease of approximately 25 % with 1000 m depth (10 MPa), which is less than the ROP decrease observed in field conditions (Wittig et al. (2015)). Thus, we claim that the RS effect of the rock cannot fully explain the ROP decrease with depth. The combined effects of RS and CHD in the case of percussive drilling, analogous to rotary drilling, remains to be investigated. During percussive drilling, the fluid activating the piston goes out of the hammer through the drill bit nozzle and flushes the rock debris to the surface, through the annulus between the borehole wall and the drill string (see Fig. 2). The cleaning action of the drilling fluid should ensure that the hammer hits new intact rock at each impact (typical frequency range: 20-50 Hz, Depouhon (2014)). When the flushing is inefficient, repeated crushing of the cuttings may occur, known as regrinding leading to further drop in ROP.

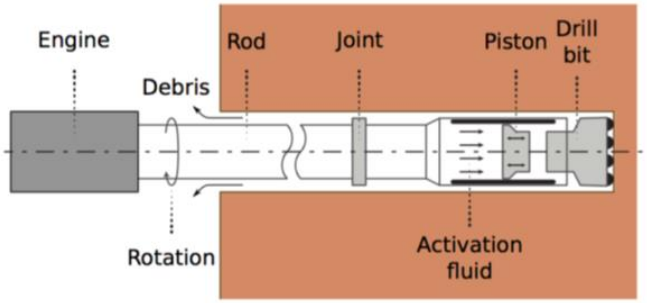

Figure 2: Sketch of down-the-hole (DTH) drilling system (from Depouhon (2014))

These observations are the basis of the theoretical analysis presented in this paper. Flushing and chip-hold-down are studied in the section about the removal of one chip. These results are used later to evaluate the ROP, where regrinding and chip size distribution are considered. In particular, we develop a simplified rock debris formation and removal model to capture the influence of the drilling parameters (fluid, impact energy and frequency) on the chip hold down effect and subsequent decrease in rate of penetration.

2. ONE CHIP REMOVAL MODEL

2.1 Description of Impact and Removal Phases

A 2D case study of fluid structure interaction is performed to investigate the evacuation of one chip by the drilling fluid. The chip is modelled as a semi-elliptical piece of rock formed during the drill bit impact and defined by its length L and its height h. The width of the problem in the third dimension is the chip thickness d. The hydrostatic pressure of the fluid p_0 is supposed to be constant, and the fluid is assumed to flow along the wall with a constant velocity U_0, which is verified far from the injection holes. The geometry of the problem is represented in Fig. 3, where e is the width of the fluid layer between the bedrock and the chip. The aim is to find the influence of fluid and drilling parameters on the evacuation of the chip from the bedrock. From the chip and fluid parameters summarized in Table 1, ten relevant parameters (and two related parameters) from three independent physical units are identified. Then at least six dimensionless parameters can be built, where the last two in Table 1 represent the Reynolds numbers of ejection and transport, respectively. Fig. 3 sketches the various steps of the chip during impact and removal. The various forces applied by the fluid on the chip is defined as follow:

- Hydrostatic pressure (vertical descendent) applied above the chip: $F_0 = p_0 dL$;
- Bernoulli lift (vertical ascendant) due to the fluid velocity above the chip: $F_B = p_B dL$ with $p_B = \frac{1}{2}\rho C_L U_0^2$;
- Viscous force (vertical descendent) of the fluid under the chip, based on the Reynolds equation for thin lubricating films: $F_{vis} = \mu \frac{dL^3}{e^3}\dot{e}$;
- Drag force (horizontal in the direction of the fluid flow): $F_D = \frac{1}{2}\rho C_D dL U_0^2$.

C_L is a lift coefficient and C_D a drag coefficient which, in principle, are dependent on chip geometry and fluid velocity.

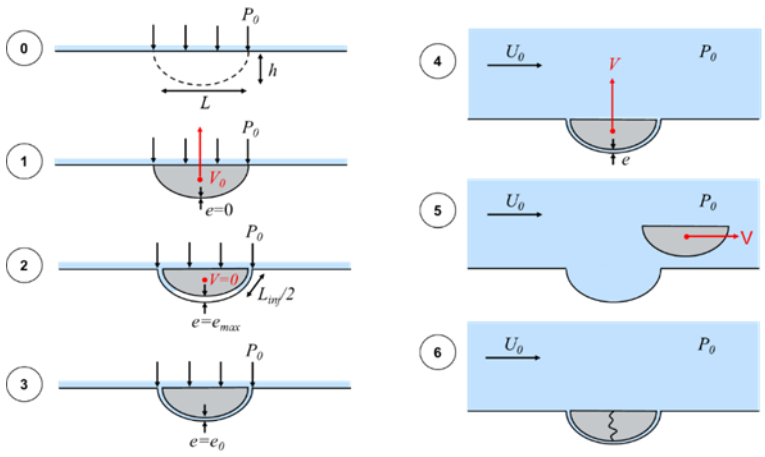

Figure 3: Chip geometry and life steps during impact and removal

Table 1: Chip, fluid and dimensionless parameters of the case

Chip parameters	Fluid parameters	Dimensionless parameters
ρ_r : density of the rock	ρ : density of the fluid	e / L
L : characteristic length	e : width of layer under chip	$\rho_r v_0^2 / p_0$
h : characteristic height	μ : dynamic viscosity	h / L
v_0 : initial velocity of the chip	ν : kinematic viscosity, $= \mu / \rho$	ρ_r / ρ
d : 3D thickness of the chip	p_0 : hydrostatic pressure	Lv_0 / ν
m : mass of the chip, $= \rho_r hdL$	U_0 : velocity above the chip	LU_0 / ν

The existence and predominance of each force evolves during the various phases of the chip removal. Phase 0 corresponds to the propagation of a crack leading to the creation of the chip. Phase 1 corresponds to the initial state of the created chip, still in contact with the bedrock, i.e. no fluid has yet infiltrated between the chip and the bedrock. At this stage, we assume that the rock chip has an ascendant vertical initial velocity that will be restrained by the hydrostatic pressure (the only force applying so far). As the fluid infiltrates under the chip during phase 2 (i.e. L_{inj} increases), we assume that the movement of the chip remains vertical. During this phase, depending on the fluid and chip properties, the chip velocity may decrease to zero and even change sign. Phase 3 corresponds to the stage where the chip is surrounded by fluid, with a layer of fluid e_0 between the chip and the bedrock. At this stage, the hydrostatic pressure F_0 does not influence on the movement of the chip anymore. Then, in phase 4, the Bernoulli lift force becomes predominant and the chip is lifted from the bedrock. The viscous force retaining the chip also applies during this phase. As the layer of fluid under the chip increases, the viscosity effect becomes negligible and the horizontal drag force will become predominant. This is the start of phase 5, in which movement of the chip along the wall is dominant. The final phase 6 illustrates the regrinding of a chip studied in Section 3.1.

Throughout the various phases (except phase 5 and 6), the general equation of the vertical movement can be written as follows:

$$\rho_r h\ddot{e} = p_u - p_a \tag{1}$$

where $\ddot{e}$ is the vertical acceleration of the chip, and p_u and p_a are the mean pressures under and above the chip, respectively. The expression for the pressures will vary during the various phases.

Phase 0-1: Chip creation and initial configuration

As seen during impact testing, some of the chips are ejected from the indented surface with a non-negligible velocity. In the Griffith theory (Griffith (1921)), it is assumed that the elastic energy of deformation is consumed by the crack opening (Anderson (2005)). Thus, in this study we assume that the kinetic energy of the chip is provided by elastic collision from the drill bit, so the conservation of momentum gives (Love (1897))

$$v_{chip} = \frac{2}{1+\frac{m_{chip}}{m_{bit}}} v_{bit} \tag{2}$$

where (m_{chip}, v_{chip}) and (m_{bit}, v_{bit}) are the mass and velocities of the chip and bit, respectively. As the chip mass is negligible compared to the mass of the drill bit, the ejection velocity of the small chips at impact can be approximated to $v_{chip}=2v_{bit}$. This was verified experimentally for small chips ejection during single impact in air atmospheric conditions (see Fig. 4). The impact of a 10 mm spherical indenter on a block of Kuru granite rock was carried out with a split Hopkinson pressure bar (SHPB) device at impact velocity $v_i=v_{it}=9$ *m/s* and a sequence of images was recorded at a frequency of 40 kHz. The ejection of debris was observed to occur from the beginning of the bit penetration at an average ejection velocity $v_{chip}=19$ *m/s*.

t = 0 ms t = 0.075 ms t = 0.15 ms

Figure 4: Impact of a 10 mm diameter spherical indenter on Kuru granite at 9 m/s

Numerical simulations of indentation show the drill bit velocity decrease during penetration inside the rock (Tuomas (2004)), so $v_{bit} \in [0, v_i]$ during the indentation phase. The elastic shock hypothesis leads to $v_{chip} \in [0, 2v_i]$, depending on when the chip is created during indentation. The larger chips are created after the crushed zone is formed under the drill bit (Tan et al. (1998)), when the drill bit velocity is smaller than the initial impact velocity v_i. Consequently, we assume here that the ejection velocity follows a linear decreasing relation with the chip size:

$$v_0(L) = \tilde{v}_0 \left(1 - \frac{L}{\tilde{L}}\right) \tag{3}$$

where $\tilde{v}_0 = v_0(L=0) = 2v_i$ is the ejection velocity of small chips and $v_0(\tilde{L}) = 0$ with $\tilde{L}$ the maximum length of chips created during indentation.

Phase 2: Fluid infiltration

Before fluid flows under the chip (phase 1), $p_u = 0$ because capillary effects can be neglected. Fluid infiltration is assumed to start as soon as the chip is created. We assume that the present issue can be treated in an analogous manner to fluid stiction with fluid infiltration between two plates (Roemer et al. (2015)), as illustrated in Fig. 5. The flow problem is symmetrical, as the fluid infiltrates from both sides of the chip. From the Bernoulli equation, an approximate injection speed is $v_{inj} = \sqrt{2p_0/\rho}$ as the pressure in the section not yet filled with fluid is zero. The conservation of the volume of fluid under the chip $V = eL_{inj}$ can be written, considering the incoming flow rate $D_e = ev_{inj}$, as

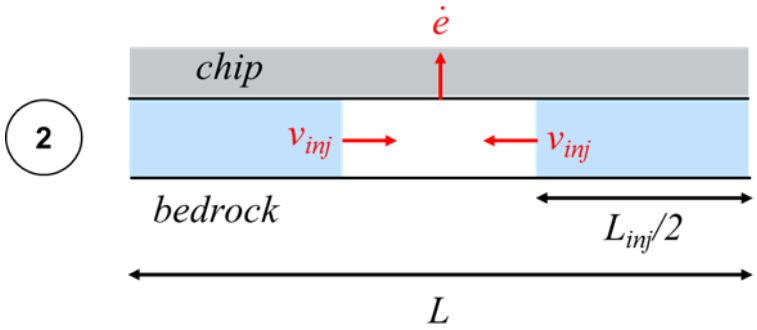

Figure 5: Close up on phase 2: idealized infiltration of the fluid between the chip and the bedrock

$$\dot{V} = D_e \quad \text{with} \quad \begin{cases} L_{inj}(t=0) = 0 \\ L_{inj}(t=t_{fill}) = L \end{cases} \tag{4}$$

where t_{fill} is the time to fill the gap beneath the chip. The mean pressure under a plate lifted with a speed $\dot{e}$ and partly filled with fluid is (Roemer et al. (2015))

$$p_u = \left[p_0 - \frac{\mu \dot{e} L_{inj}^2}{2e^3} \right] \frac{L_{inj}}{2L} \tag{5}$$

where the total length of the injection zone $L_{inj} \in [0, L]$. With $p_a = p_0 - p_B \approx p_0$, Eq. (1) with initial conditions becomes

$$\rho_r h \ddot{e} = p_u - p_0 = -p_0 \left(1 - \frac{L_{inj}}{2L}\right) - \frac{\mu \dot{e} L_{inj}^3}{4e^3 L} \quad \text{with} \quad \begin{cases} \dot{e}(0) = v_0 \\ e(0) = 0 \end{cases} \tag{6}$$

An injection time scale is defined by

$$\tau_{inj} = \frac{L}{v_{inj}} = L\sqrt{\frac{\rho}{2p_0}} \tag{7}$$

The fluid-structure interaction problem is solved by combining Eq. (4) and Eq. (6), which is rendered dimensionless by the transformations $\bar{t} = t/\tau_{inj}$, $x = e/(\tau_{inj} v_0)$, $y = L_{inj}/L$, $z = \dot{e}/v_0$ to the system

$$\begin{aligned} \dot{x} &= z \\ \dot{y} &= 1 - \frac{yz}{x} \\ \dot{z} &= -A\left(1 - \frac{y}{2} + B\frac{zy^3}{x^3}\right) \end{aligned} \quad \text{with} \quad \begin{aligned} x(0) &= 0 \\ y(0) &= 0 \\ z(0) &= 1 \end{aligned} \tag{8}$$

where the notation $\dot{x}$ means $dx/d\bar{t}$ and the expressions for the parameters are

$$\begin{aligned} A &= \frac{p_0\tau_{inj}}{\rho_r h v_0} = \frac{L}{\rho_r h v_0}\sqrt{\frac{\rho p_0}{2}} \\ B &= \frac{\mu}{2\rho\tau_{inj}v_0^2} \end{aligned} \tag{9}$$

The ending condition is $L_{inj}(t_{fill}) = L$ or, expressed in the transformed variable, $y(\bar{t}_{fill}) = 1$. The parameter A can also be seen as a ratio between time scales $A = \tau_{inj}/\tau_{chip}$, where $\tau_{chip} = \rho_r h v_0/p_0$. Fig. 6 gives the solution of the dimensionless system for three values of A, and B set equal to 0.1. It appears that the gap between the chip and the bedrock, e, can either monotonically increase (for $A<A_c$) or have a parabolic shape (for $A>A_c$). These results are interpreted as a condition of evolution of the chip:

$$\begin{cases} A < A_c \Leftrightarrow \tau_{inj} < \tau_{chip} A_c : \text{ fluid injection faster than chip kinetic energy absorption, chip is ejected} \\ A = A_c \Leftrightarrow \tau_{inj} = \tau_{chip} A_c : \text{ ejection and fluid injection compensate so } \dot{e} = 0 \text{ and } e_{fill} = e_{max} \text{ at } t_{fill} \\ A > A_c \Leftrightarrow \tau_{inj} > \tau_{chip} A_c : \text{ chip fall back against bedrock before fluid injection is finished} \end{cases} \tag{10}$$

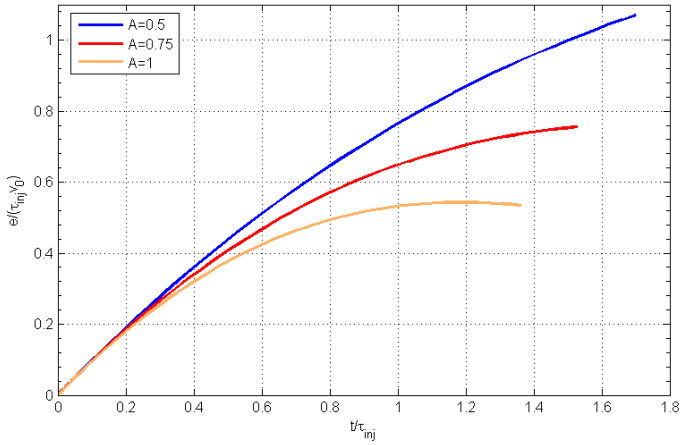

Figure 6: Phase 2 - Dimensionless fluid layer thickness vs. time for various values of *A* at *B*=0.1

The value of the critical parameter A_c lies in the range 0.85-0.89 for small values of B (≤ 0.1). Fig. 7 shows how the value of A_c varies with B. Note also that t_{fill} varies with A and B, as does the gap distance when the gap is completely filled with liquid, e_{fill}, and the maximum gap, e_{max} (see Fig. 8). The parameter A can also be expressed as a ratio of pressures:

$$A = \frac{\tau_{inj}}{\tau_{chip}} = \sqrt{\frac{p_0}{p_{chip}}} \quad \text{with} \quad p_{chip} = 2\frac{\rho_r^2 v_0^2}{\rho}\left(\frac{h}{L}\right)^2 \tag{11}$$

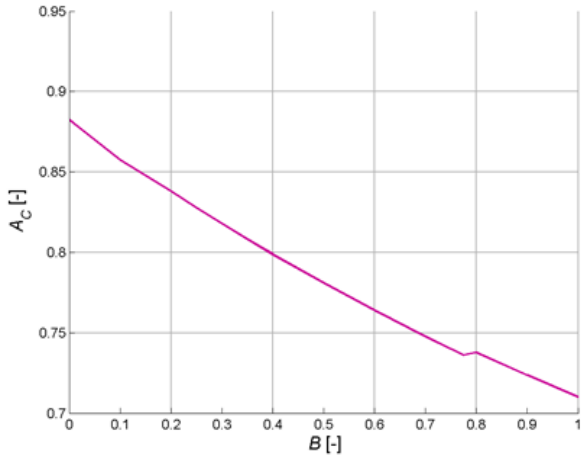

Figure 7: Phase 2 – Value of critical parameter A_c vs. parameter B

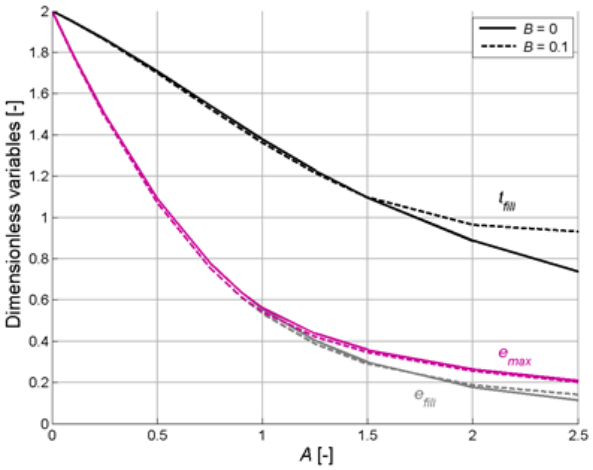

Figure 8: Phase 2 - Dimensionless variables (t_{fill}, e_{fill}, and e_{max}) vs. parameter A (for two values of B)

where the critical pressure under which the chip is ejected is expressed as $p_{chip} = p_0 A_c^{-2}$. When $\tau_{inj} > \tau_{chip} A_c$, the chip falls back in the direction of the bedrock after reaching a maximum height. The thickness of the fluid layer between the chip and the bedrock is of interest to evaluate later when viscous effects apply. This thickness can be evaluated at $t = t_{fill}$, and it is seen that its dimensionless value multiplied by A is approximately constant (~ 0.5), for $0.25 < A < 1.5$. Therefore, we can establish the following relation:

$$\frac{e_{fill}}{L} \sim \frac{\rho_r v_0^2 h}{2 p_0 L} \tag{12}$$

Phase 3-4: Chip lift with fluid stiction

At the end of the fluid infiltration, when $L_{inj} = L$, the hydrostatic forces vanish since the fluid surrounds the chip. Consequently, the Bernoulli pressure and viscous effects are not negligible anymore with $p_a = -p_B$ and $p_u = -\mu \dot{e} L^2 / e^3$. Thus, Eq. (1) becomes

$$\rho_r h \ddot{e} = -\mu \dot{e} \frac{L^2}{e^3} + p_B \quad \text{with} \quad \begin{cases} \dot{e}(t=0) \sim 0 \\ e(t=0) = e_{fill} \end{cases} \tag{13}$$

where $t = 0$ at the beginning of the viscous phase and the velocity is assumed negligible. The solution of this equation is shown in Fig. 9 for different values of the parameter E defined as

$$E = \frac{p_B \tau_{vis}^2}{\rho_r h e_{fill}} \quad \text{where} \quad \tau_{vis} = \frac{\mu}{2 p_B} \left(\frac{L}{e_{fill}} \right)^2 \tag{14}$$

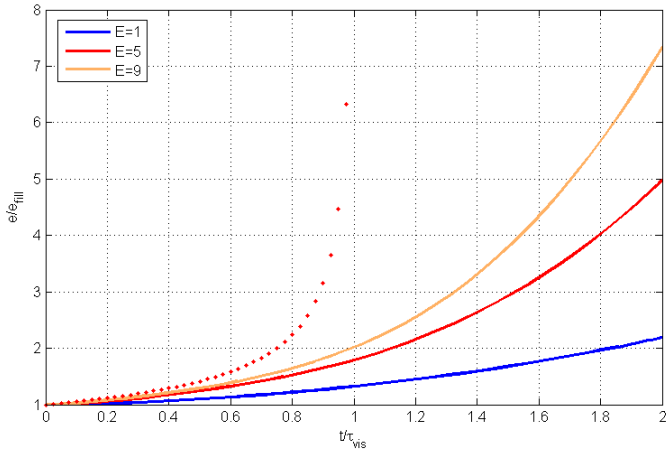

Figure 9: Idealized Bernoulli lift vs. time for a chip with different physical properties and initial conditions (*E* parameter)

A simplified solution is obtained by neglecting the acceleration ($E \to \infty$). The analytical solution is then

$$e(t) = e_{fill}\left(1 - \frac{t}{\tau_{vis}}\right)^{-1/2} \tag{15}$$

This solution is shown as the dotted curve in Fig. 9. From Eq. **Error! Reference source not found.** and Eq. (14), the characteristic time can be explicated as

$$\tau_{vis} \sim \frac{2\mu}{p_B}\left(\frac{p_0}{\rho_r v_0^2}\right)^2 \left(\frac{L}{h}\right)^2 \tag{16}$$

Phase 5: Chip transport along the borehole

The takeaway of the chip by the flow is studied by assuming that the chip is subjected to a drag force $F_D = \frac{1}{2}\rho C_D d L \tilde{U}_0^2$ with $\tilde{U}_0$ the relative velocity of the chip in the flow. The equation of the movement of the chip is

$$\rho_r L \ddot{x} = \frac{1}{2}\rho C_D \left(U_0 - \dot{x}\right)^2 \quad \text{with} \quad \begin{cases} x(t=0) = 0 \\ \dot{x}(t=0) = 0 \end{cases} \tag{17}$$

where the time is zero at the beginning of this transport phase. The solution of this equation is

$$x(t) = U_0 \tau_D \left[\frac{t}{\tau_D} - \ln\left(1 + \frac{t}{\tau_D}\right)\right] \quad \text{with} \quad \tau_D = \frac{2\rho_r L}{\rho C_D U_0} \tag{18}$$

This phase is assumed to last until the chip has reached the annulus of the borehole. This corresponds to $x\left(t = t_f\right) = R_{bit}$.

2.2 Characteristic Times Summary

The evolution phases described in Section 2.1 is summarized into the main phenomena: fluid injection, fluid stiction (with viscous effects) and horizontal drag flow. The characteristic times associated to the three phenomena are summarized in Table 2, together with order of magnitude, equation of movement and main hypothesis. It appears that the characteristic time predicted by numerical simulations is of the same order as the analytical model. Moreover, the effects of fluid viscosity and velocity U_0 on the numerical characteristic times are in the same order as in the analytical model.

Table 2: Chip removal mechanisms, characteristic times and order of magnitudes

Phase	Characteristic time	Order of magnitude
Injection	$\tau_{inj} \sim \tau_{chip} = \frac{\rho_r h v_0}{p_0}$	$\tau_{chip} \sim 10^{-4} s$
Stiction	$\tau_{vis} \sim \frac{2\mu}{p_B}\left(\frac{p_0}{\rho_r v_0^2}\right)^2 \left(\frac{L}{h}\right)^2$	$\tau_{vis} \sim 10^{-3} s$
Drag (transport)	$\tau_D = \frac{2\rho_r L}{\rho C_D U_0}$	$\tau_D \sim 10^{-2} s$

3. REGRINDING CRITERION AND CHIP SIZE DISTRIBUTION

The characteristic times of removal of one chip with a given geometry (h, L) are now used to evaluate the influence of chip-hold-down (CHD) on ROP. We achieve this by using the above results as a regrinding condition applied to a statistical distribution of chip size and shape.

3.1 Phase 6: Regrinding Criterion

During percussive drilling, when a rock chip is not removed efficiently from the bedrock after impact, chip hold down occurs. In this study, we consider that regrinding happens (phase 6) if the chip has not reached the transport phase (phase 5) when a second impact occurs. The reason for this assumption is that between two impacts, the drill bit is generally resting and rotating upon the bedrock (Depouhon (2014)). Thus, if a chip is in the transport phase, there is few chances that a button will impact it a second time. Consequently, the condition for good chip evacuation process can be written $\tau_{CHD} \leq T_f$ where $\tau_{CHD} = \tau_{inj} + \tau_{vis} \sim \tau_{vis}$ is the chip hold down time of the cleaning process (excavation of the chip), and $T_f = 1/f$ is the time between two impacts of the drill bit. If $\tau_{CHD} > T_f$, we postulate that regrinding occurs. Then, we assume that the second impact will not lead to indentation and chipping. Besides, we neglect any further regrinding of the actual chip, i.e. regrinding can occur only once. As a result, a chip that is subjected to regrinding needs twice as much time to be evacuated. From Eq. (10) and Eq. (16), which gives τ_{vis} as a function of p_0, the regrinding condition can also be written as a condition on fluid pressure and chip geometry:

$$\tau_{CHD} \leq T_f \quad \Leftrightarrow \quad p_0 \leq p_{CHD} \quad \text{with} \quad \begin{cases} p_{CHD} = \tilde{p}_{CHD}\left(1-\dfrac{L}{\tilde{L}}\right)^2 \dfrac{h}{L} \\ \tilde{p}_{CHD} = \rho_r \tilde{v}_0^2 \left(\dfrac{p_B T_f}{2\mu}\right)^{1/2} \end{cases} \tag{19}$$

where the reference chip hold down pressure $\tilde{p}_{CHD}$ depends on the chip geometry through the Bernoulli lift pressure p_B. Here, however, it is assumed a constant lift coefficient $C_L = 1$, which implies that the Bernoulli pressure does not depend on the chip geometry (at the zero order).

3.2 Chip Size Distribution

In real drilling conditions rock chips have various shapes and sizes (Nas et al. (2010)). One limitation on the observation of the chips size after transport to the surface is that the distribution observed takes into account regrinding. In other words, it does not necessarily correspond to the size distribution at the creation of the chips. Moreover, the importance of chip size and shape distribution was highlighted in a study on chip removal with hydraulic jet (Cheatham and Yarbrough (1964)). Generally hard rock chips are rather flat (Johnson (1995)), and in particular in percussive drilling flat disk-shaped cuttings were observed by Han and Bruno (2006). Consequently, flat chip distributions are considered in the evaluation of the ROP.

3.3 Rock Strengthening (RS) and Chip Hold Down (CHD) Effects

During percussive drilling regrinding of the chip will lead to decreased efficiency. Since the rock strengthening effect is too small to explain the ROP decrease observed in field conditions, empirical formula for the effect of CHD on ROP were proposed in the case of roller cone drilling (Zhu et al. (2014)). Similarly, in this study, the ROP decrease due to the chip hold down effect (regrinding) is applied as a corrective factor, ϕ_{CHD}, on a ROP function accounting for rock strengthening, ϕ_{RS}, through the expression:

$$ROP = ROP_0 \, \phi_{RS} \, \phi_{CHD} \tag{20}$$

The RS effect can be approximated by a linear decrease with respect to hydrostatic pressure as long as the pressure is fairly small

$$\phi_{RS} = 1 - \alpha_{RS} p_0 \tag{21}$$

where α_{RS} = 0.0125 MPa^{-1} is the slope of the ROP curve calibrated from p_0 = 0 – 20 MPa, i.e. between surface and 2 km depth (Saksala (2016)). This value is for percussive drilling in granite, while for rotary drilling in sedimentary rocks a value of α_{RS} = 0.0288 MPa^{-1} can be approximated (see Fig. 1a). The CHD factor for regrinding is defined as the average fraction of a chip removed per impact, as

$$\phi_{CHD} = \langle n \rangle \quad \text{with} \quad n = \begin{cases} 1 & \text{if } p_0 < p_{CHD} \\ \frac{1}{2} & \text{if } p_0 \geq p_{CHD} \end{cases} \tag{22}$$

The average of n is then a function of chip size and shape distribution through the probabilities

$$\langle n \rangle = \mathbf{P}\left(p_0 < p_{CHD}\right) + \frac{1}{2}\mathbf{P}\left(p_0 \geq p_{CHD}\right) = 1 - \frac{1}{2}\mathbf{P}\left(p_0 \geq p_{CHD}\right) \tag{23}$$

and is interpreted as the normalized number of chips removed per hit. The two limiting cases are:

- Under atmospheric conditions: $p_0 = p_{atm}$ so the condition $p_0 < p_{CHD}$ is fulfilled for almost all chips and consequently $\langle n \rangle \sim 1$, $ROP = ROP_0 \, \phi_{RS}$.
- At very large depth: $p_0 \geq p_{CHD}$ for almost all chips, $\langle n \rangle \sim 1/2$ and $ROP = \frac{1}{2} ROP_0 \alpha_{RS}$.

3.4 Evaluation of Rate of Penetration (ROP)

For each chip of a given distribution, the first condition to test is the ejection, i.e. Eq. (10) and Eq. (11). The second condition to test is the chip hold down, i.e. Eq. (19). Indeed, it appears that for water only the second condition is necessary since $p_{chip} < p_{CHD}$. The link between hydrostatic pressure, p_0, and depth, z, is given by $p_0 = p_{atm} + \rho g z$ for a column of fluid (g is the gravitational acceleration). This will be used to plot the results from the analysis of the influence of pressure on *ROP*. The size and the shape of the chips are assumed to follow a distribution with $L/\tilde{L} \in [0;1]$ and $\beta h/L \in [0;1]$ with a shape parameter $(h/L)_{\max} = 1/\beta$. To evaluate the probability given in Eq. (23), we introduce a transformed variable

$$1 - \frac{L_0}{\tilde{L}} = \sqrt{\frac{\beta p_0}{\tilde{p}_{CHD}}} \tag{24}$$

and utilize that $p_0 \geq p_{CHD} \quad \Leftrightarrow \quad \frac{\beta p_0}{\tilde{p}_{CHD}} \geq \left(1 - \frac{L}{\tilde{L}}\right)^2 \frac{\beta h}{L}$. Then, for uniform distributions of $L/\tilde{L}$ and $\beta h/L$, the probability can be expressed as

$$\mathbf{P}\left(p_0 \geq p_{CHD}\right) = \int_0^{\frac{L_0}{\tilde{L}}} \left(\frac{1 - \frac{L_0}{\tilde{L}}}{1 - \frac{L}{\tilde{L}}}\right)^2 d\left(\frac{L}{\tilde{L}}\right) + \int_{\frac{L_0}{\tilde{L}}}^{1} d\left(\frac{L}{\tilde{L}}\right) = \left(1 - \frac{L_0}{\tilde{L}}\right)\left[2 - \left(1 - \frac{L_0}{\tilde{L}}\right)\right] = \sqrt{\frac{\beta p_0}{\tilde{p}_{CHD}}}\left(2 - \sqrt{\frac{\beta p_0}{\tilde{p}_{CHD}}}\right) \tag{25}$$

when $\beta p_0 / \tilde{p}_{CHD} \leq 1$. When this ratio is larger than unity, the probability will be unity. The chip hold down factor can then be written as

$$\phi_{CHD} = \begin{cases} 1 - \sqrt{\frac{\beta p_0}{\tilde{p}_{CHD}}} + \frac{\beta p_0}{2\tilde{p}_{CHD}} & \text{for} \quad \frac{\beta p_0}{\tilde{p}_{CHD}} \leq 1 \\ \frac{1}{2} & \text{for} \quad \frac{\beta p_0}{\tilde{p}_{CHD}} > 1 \end{cases} \tag{26}$$

The choice of size distribution affects the evolution of the regrinding factor with depth, as shown in Fig. 10, where the stochastic regrinding factor is given for uniform and normal distributions. Fig. 11 provides the normalized ROP prediction from Eq. (21) and Eq. (23) for several values of β. Table 3 shows the parameter values applied in these graphs. A good fit with field data is obtained for $\beta = 4$. From a sensitivity analysis of Eq. (19), we see that the influence of fluid velocity and viscosity is weaker than the influence of the impact velocity:

$$\frac{d(\tilde{p}_{CHD}/\beta)}{\tilde{p}_{CHD}/\beta} = 2\frac{dv_0}{v_0} + \frac{dU_0}{U_0} + \frac{1}{2}\frac{dT_f}{T_f} - \frac{1}{2}\frac{d\mu}{\mu} - \frac{d\beta}{\beta} \tag{27}$$

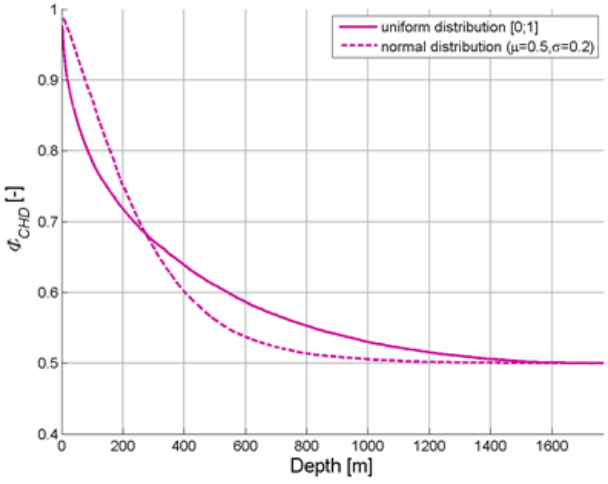

Figure 10: Regrinding factor vs. depth with uniform and normal chip distributions ($\beta = 4$)

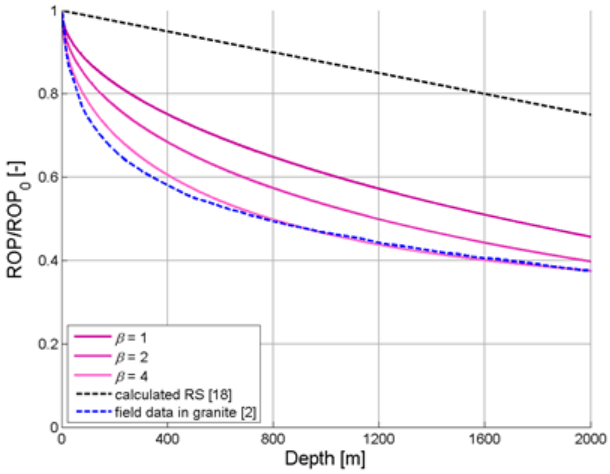

Figure 11: Normalized ROP vs. depth with uniform chip distribution and various chip geometries (Ref 2 = Wittig et al. (2015), ref 18= Altindag (2004))

Table 3: Parameter values for chip hold down factor and rate of penetration

Impact frequency f [Hz]	Ejection velocity $\tilde{v}_0$ [m/s]	Fluid velocity U_0 [m/s]	Rock density ρ_r [kg/m^3]
50	10	5	2000

Table 4 provides the different critical pressures of the model and corresponding critical depth, for different fluids. It appears that the critical pressures with air corresponds to a depth of 56 km, which suggests that the chip hold down effect is not substantial with air percussion drilling. The ROP decrease observed with air percussion drilling in Fig. 11 is mostly related to water infiltration into the well and cuttings transport problems (Wittig et al. (2015)). Those results are in agreement with existing literature statements, as for example for rotary drilling: "The properties of drilling fluids that affect the penetration rate are density, filtration properties, viscosity, solids content, and size distribution. The most critical property is density. [...] The generalizations that air drills faster than water and water drills faster than mud are confirmed by years of experience." (Roscoe Moss Company (2008))

Table 4: Comparison of critical pressures and depths for different fluids ($\beta = 4$)

Fluid	ρ [kg/m^3]	μ [Pa s]	$\langle p_{chip} \rangle$ [MPa]	z_{chip} [km]	$\langle p_{CHD} \rangle$ [MPa]	z_{CHD} [km]
Water	1000	10^{-3}	0.006	0	2.95	0.29
Mud	1200	$24 \cdot 10^{-3}$	0.005	0	0.66	0.047
Air	1.2	$1.8 \cdot 10^{-5}$	4.63	385	0.76	56

Empirical models for rotary drilling are proposed in the literature to account for chip hold down effect in addition to the drop of ROP induced by rock strengthening, as for instance Zhu et al. (2014)

- $ROP = ROP_0 e^{-A\Delta p}$ where Δp is the differential bottom hole pressure and A is a coefficient related to the rock properties.
- $ROP = \left(B f_{CHD}(\Delta p) + C \right)^{-1}$ where B is a coefficient related to rock and drilling parameters and C is a coefficient related to the fluid parameters (in particular the fluid viscosity).

Note that these results consider rocks with pore pressure, where static chip hold down effect keeps the cuttings stuck by differential pressure (overbalanced drilling conditions).

4. CONCLUSIONS AND PERSPECTIVES

The removal of one chip is treated as a 2D fluid-structure interaction problem, in the case of impermeable rock and incompressible drilling fluid. After the chip creation, several steps of the cleaning process are assumed: (i) vertical chip ejection, (ii) vertical chip lift with stiction, and (iii) horizontal transport towards the annulus. The characteristic times associated with each step are evaluated analytically and used to predict the evolution of rate of penetration (ROP) with depth, in percussive drilling. This is achieved by

- Establishing a physically based criterion for chip hold down effect (CHD) and subsequent regrinding (repetition of impact on the same chip). This criterion compares the hydrostatic pressure with a critical chip hold down pressure that depends on chip geometry, fluid properties, and impact frequency.
- Based on in-field debris observation, a statistical representation of chip distribution (size and shape) is introduced. The CHD criterion is applied to the chip distribution, leading to a pressure dependent regrinding factor (percentage of regrinding).

- Assuming the decrease of ROP with depth is a multiplication of rock strengthening (RS) and chip hold down effects, where the RS effect is taken from the literature.

An analytical solution for ROP is calculated for a uniform chip distribution and the main conclusions of the study are:

- The characteristic times of each cleaning steps depend on fluid properties (pressure, density, viscosity, initial velocity) and chip parameters (geometry, density, velocity).
- The most influential parameters on ROP evolution with depth are the hydrostatic pressure (i.e. fluid density), the chip geometry and the drill bit velocity. The fluid viscosity and velocity have a less substantial effect.
- Accounting for both rock strengthening (RS) and chip-hold down (CHD) effects enable to reproduce a realistic decay of ROP with depth.

In agreement with literature results (Roscoe Moss Company (2008)), our results show that the CHD effect can be avoided by decreasing the density of the fluid and subsequent borehole pressure, i.e. using underbalanced drilling conditions. However, overbalanced conditions are privileged in deep drilling for more stability of the well bore according to Kollé (2000). Therefore, several methods to reduce the pressure only locally are currently under development. Vortex and reverse flow drill bits use the venturi effect to decrease the pressure under the drill bit (Zhu et al. (2014), Nas et al. (2010)). Although innovations described here are generally designed for ductile soft rocks, the chip hold down also affects the hard rock removal so these could be investigated for hard brittle formations as well. The conclusions above can seem somewhat contradictory with available literature results that emphasize the importance of fluid viscosity (Judzis et al. (2009)). The conclusion of the present study comes from the mathematical sensitivity analysis and does not account for the real possibility to vary the drilling parameters. Indeed, it is possible to vary the viscosity of the fluid greatly, while it is more difficult to vary the drill bit velocity, for instance. The conclusions of this study are therefore not in contradiction with available experimental parametrical studies. Further, the study proposed here relies on several assumptions that could be discussed:

- The vertical direction of initial velocity of the chip and movement of the chip during infiltration and stiction
- The possible mechanical contact between the bit and the chip is also neglected. Indeed, the rotation per minute (RPM) of the hammer provides a horizontal movement of the drill bit which, with contact and friction with the bedrock, could contribute to the cleaning.
- The characteristic time of crack propagation responsible for the formation of the rock chip (phase 0) is neglected here, as well as the cleaning of rock powder generated by grinding (rock material right under the indenter).
- In turn, the influence of rock strengthening (or depth) on chip size distribution is not accounted for. It can be expected that the chipping process is decreased with confining pressure, due to higher rock strength and ductility.

The theoretical approach supported by experimental validation would be helpful to provide further fundamental understanding of the CHD effect. Perspectives to further validate the assumptions of this theoretical approach are suggested below:

- Verify that regrinding is responsible for ROP decrease with depth in percussive drilling by analyzing cuttings from the field. Indeed, the chip size distribution with depth analysis should show some decrease of the mean chip length.
- Impact tests carried out in fluid and instrumented with high speed camera could provide data about the chip ejection (or chip-hold down). The influence of fluid pressure on the chip removal could also be studied in a pressure chamber to capture the effect of depth.

Overall, this study provides a parametric tool for sensitivity analysis that could support innovative tools development and the choice of fluid and operating conditions.

Acknowledgements

The financial support from the Research Council of Norway and the industrial partners involved in the INNO-Drill project (grant number 254984) is gratefully acknowledged.

REFERENCES

Altindag, R.: Evaluation of drill cuttings in prediction of penetration rate by using coarseness index and mean particle size in percussive drilling, Geotechnical and Geological Engineering, 22 (3), (2004), 417-425.

Andersen, E.E., Maurer, W.C., Hood, M., Cooper, G., and Cook, N.: Deep drilling basic research, Volume 5 - System Evaluations, Final Report, Gas Research Institute, Chicago, Illinois, (1990), GRI-90/0265.5.

Anderson, T.L.: Fracture mechanics: fundamentals and applications, 3rd ed., Boca Raton, Florida, CRC Press (2005).

Cheatham Jr, J.B., and Yarbrough, J.G.: Chip Removal by a Hydraulic Jet, SPE Journal, 4 (1), (1964), 21-25.

Depouhon, A.: Integrated dynamical models of down-the-hole percussive drilling, Doctoral thesis, University of Minnesota, Minneapolis, Minnesota (2014).

Finger, J., and Blankenship, D.: Handbook of best practices for geothermal drilling, Sandia National Laboratories (2010).

Fourmeau, M., Depouhon, A., Kane, A., Hoang, H., and Detournay, E.: Influence of indexation and impact energy on bit/rock interface law in percussive drilling: an experimental study, Proceedings, 49th U.S. Rock Mechanics/Geomechanics Symposium, San Francisco, California (2015), ARMA-2015-522.

Garnier, A.J., and Van Lingen, N.H.: Phenomena affecting drilling rates at depth, Petroleum Transactions AIME, 216, (1959), 232-239.

Griffith, A.A.: The phenomena of rupture and flow in solids, Philosophical Transactions of the Royal Society of London, A, 221, (1921), 163–198.

Han, G., and Bruno, M.: Percussion drilling: from laboratory tests to dynamic modeling, Proceedings, International Oil & Gas Conference and Exhibition, Beijing, China (2006).

Hareland, G., and Hoberock, L.L.: Use of drilling parameters to predict in-situ stress bounds, Proceedings, SPE/IADC Drilling Conference, Amsterdam, The Netherlands, (1993), SPE-25727-MS.

Hoek, E., and Brown, E.E.: Underground excavation in rock, Institution of Mining and Metallurgy, London: E&FN Spon (1980).

IEA. Technology roadmap - geothermal heat and power. http://www.iea.org/roadmaps/, (2011) (accessed 2017-06-02).

Johnson, P.W.: Design techniques in air and gas drilling: cleaning criteria and minimum flowing pressure gradients, J Canadian Petroleum Technology, 34 (5), (1995), 18-26.

Judzis, A., Black, A.D., Curry, D.A., Meiners, M.J., Grant, T., and Bland, R.G.: Optimization of deep-drilling performance--Benchmark testing drives ROP improvements for bits and drilling fluids, SPE Drilling & Completion, 24 (1), (2009).

Kollé, J.J.: Increasing drilling rate in deep boreholes by impulsive depressurization, Proceedings, 4th North American Rock Mechanics Symposium, Seattle, Washington (2000).

Love, A.E.H.: Principles of Dynamics, Cambridge University Press (1897).

Mitchell, R.F.: Petroleum engineering handbook, Volume II: Drilling engineering, Society of Petroleum Engineers (2007).

Nas, S.W., Gala, D.M., and Cox, P.: Deep air drilling application to enhance rate of penetration in extremely hard, abrasive and high temperature environment, Proceedings, International Oil and Gas Conference and Exhibition, Beijing, China (2010), SPE-132048-MS.

Niu, D.: Percussion Rock Drilling Bit with More Efficient Flushing, US Patent No. US 20100108398A1 (2010).

Rastegar, M., Hareland, G., Nygaard, R., and Bashari, A.: Optimization of multiple bit runs based on ROP models and cost equation: A new methodology applied for one of the Persian gulf carbonate fields, Proceedings, IADC/SPE Asia Pacific Drilling Technology, Jakarta, Indonesia, (2008), SPE-114665-MS.

Roemer, D.B., Johansen, P., Pedersen, H.C., and Andersen, T.O.: Fluid stiction modeling for quickly separating plates considering the liquid tensile strength, J Fluids Engineering, Trans. of ASME, 137 (6), (2015), 061205.

Roscoe Moss Company: Handbook of ground water development, Ed. John Wiley & Sons (2008).

Saksala, T.: Numerical study of the influence of hydrostatic and confining pressure on percussive drilling of hard rock, Computers and Geotechnics, 76, (2016), 120-128.

Smith, J.R.: Addressing the problem of PDC bit performance in deep shales, IADC/SPE Asia Pacific Drilling Technology, Jakarta, Indonesia, (1998), SPE-47814-MS.

Tan, X.C., Kou, S.Q., and Lindqvist, P.A.: Application of the DDM and fracture mechanics model on the simulation of rock breakage by mechanical tools, Engineering Geology, 49 (3-4), (1998), 277-284.

Tuomas, G.: Water powered percussive rock drilling: process analysis, modelling and numerical simulation, Doctoral thesis, Luleå University of Technology, Sweden (2004).

Warren, T.M.: Penetration Rate Performance of Roller Cone Bits, SPE Drilling Engineering, 2, (1987), 9-18.

Wittig, V., Bracke, R., Hyun-Ick, Y.: Hydraulic DTH fluid/mud hammers with recirculation capabilities to improve ROP and hole cleaning for deep, hard rock geothermal drilling, Proceedings, World Geothermal Congress, Melbourne, Australia (2015).

Zhu, H.Y., Liu, Q.Y., and Wang, T.: Reducing the bottom-hole differential pressure by vortex and hydraulic jet methods, J Vibroengineering, 16 (5), (2014), 2224-2249.